RESEARCH ARTICLE

QUANTUM OPTICS

Single-plasmon interferences

Marie-Christine Dheur,[1] Eloïse Devaux,[2] Thomas W. Ebbesen,[2] Alexandre Baron,[3] Jean-Claude Rodier,[1] Jean-Paul Hugonin,[1] Philippe Lalanne,[4] Jean-Jacques Greffet,[1] Gaétan Messin,[1] François Marquier[1]*

10.1126/sciadv.1501574

Surface plasmon polaritons are electromagnetic waves coupled to collective electron oscillations propagating along metal-dielectric interfaces, exhibiting a bosonic character. Recent experiments involving surface plasmons guided by wires or stripes allowed the reproduction of quantum optics effects, such as antibunching with a single surface plasmon state, coalescence with a two-plasmon state, conservation of squeezing, or entanglement through plasmonic channels. We report the first direct demonstration of the wave-particle duality for a single surface plasmon freely propagating along a planar metal-air interface. We develop a platform that enables two complementary experiments, one revealing the particle behavior of the single-plasmon state through antibunching, and the other one where the interferences prove its wave nature. This result opens up new ways to exploit quantum conversion effects between different bosonic species as shown here with photons and polaritons.

INTRODUCTION

The production of the first single-photon states (*1*, *2*) and the first demonstration of trapping of a single ion (*3*) in the early 80s marked the beginning of a long-standing effort to control and manipulate individual quantum systems. Potential applications require developing new platforms to engineer interaction between them at the nanoscale. Recent advances in the generation of optical nonlinearities at the level of individual photons (*4*) and in the interfacing of atoms with guided photons (*5*) clearly demonstrate the benefits of subwavelength confinement of the electromagnetic field. Because plasmonics provides new platforms to concentrate light to scales below that of conventional optics, plasmonic devices are excellent candidates for on-chip operations at the quantum level (*6*). Plasmons, as well as surface plasmons, are collective excitations of fermions, which are not, strictly speaking, bosons, although their commutation relations can be approximated by bosonic commutation relations with an error that decays as the inverse of the number of electrons (*7*). The quantized electric field operator for surface plasmon polaritons (SPPs) has been derived by numerous authors (*8*–*10*). As a result, SPPs are expected to behave like photons to a high degree of accuracy. The bosonic quantum nature of the plasmons has been demonstrated by several observations that reveal specific quantum features, such as coupling between a quantum emitter and a surface plasmon (*11*, *12*), preservation of quantum correlations such as entanglement and squeezing through surface plasmon channels (*13*–*17*), control of spontaneous emission of an emitter by plasmonic structures (emission direction and lifetime) (*18*, *19*), and quantum interferences (*20*–*24*). In Kolesov *et al.* (*12*), wave-particle duality of plasmons has been inferred from the observation of antibunching and spectral properties of the light coming out of a nanorod through a plasmonic channel and emitted by a single emitter coupled to it. Here, we investigate the dual wave-particle nature of the SPP along the same lines as the single-photon interferences textbook experiment by Grangier *et al.* (*1*) and Loudon (*25*). We propose the first direct measurement of the wave-particle duality for single SPP, using a true plasmonic beam splitter (BS) for SPP freely propagating on a flat gold-air interface. We generate a single SPP state by sending a photon from a single-photon source onto a photon-to-SPP coupler. A plasmonic BS is used to separate the flux of SPPs into two spatial modes, allowing the analysis of the SPP features using either a Hanbury Brown and Twiss (HBT) setup or a Mach-Zehnder (MZ) interferometer. The detection of anticorrelated events after the plasmonic BS unambiguously provides the which-path information, hence revealing the particle nature of the single SPP in the HBT configuration (*26*), whereas the wave behavior of the SPP is demonstrated in the MZ configuration with single SPPs. In addition, we observe that the presence of losses in the BS modifies the lossless MZ output signals, following the predictions made by Barnett *et al.* (*27*).

RESULTS

Single surface plasmon experiment

Because the photon-number statistics are preserved through the coupling of a photonic mode to a plasmonic mode (*8*), we used a single-photon source and an SPP-photon coupler to produce single SPPs. The single-photon source is a heralded single-photon source delivering two outputs, a single photon at 806 nm with a spectral bandwidth of $\Delta\lambda$ = 1 nm and its heralding electronic pulse. More details about the source can be found in section S1. The manipulation of the SPPs is performed on the plasmonic chip shown in Fig. 1B. This chip has been designed with in-house electromagnetic software based on the aperiodic Fourier modal method (*28*). It consists of two unidirectional plasmon launchers, a plasmon splitter, and two large strip slits that decouple the SPPs toward the rear side of the sample. All components are fabricated in a single chip by focused ion beam lithography on a 300-nm-thick gold film sputtered on top of a SiO_2 substrate. Single photons that are impinging from the front side of the chip are first converted into single SPPs via asymmetric 11-groove gratings (shown in Fig. 1A). The latter have been designed

[1]Laboratoire Charles Fabry, Institut d'Optique, CNRS, Université Paris-Saclay, 91127 Palaiseau Cedex, France. [2]Institut de Science et d'Ingénierie Supramoléculaire, CNRS, Université de Strasbourg, 67000 Strasbourg, France. [3]Centre de Recherche Paul Pascal, CNRS, 33600 Pessac, France. [4]Laboratoire Photonique, Numérique et Nanosciences, Institut d'Optique, CNRS, Université de Bordeaux, 33400 Talence, France.
*Corresponding author. E-mail: francois.marquier@institutoptique.fr

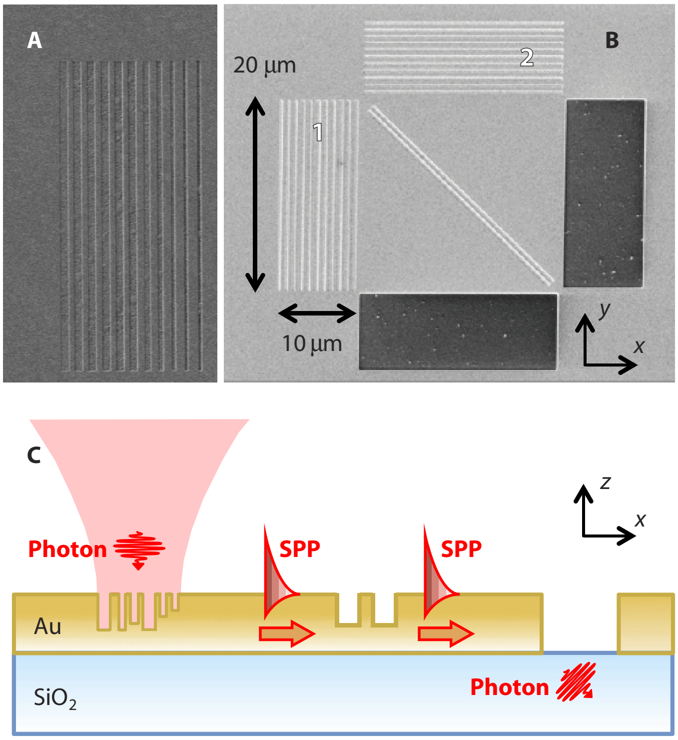

Fig. 1. The plasmonic platform. (**A**) Scanning electron microscope top view of the photon-to-SPP launcher. It is made of 11 grooves of asymmetric dimensions (*29*). (**B**) Scanning electron microscope top view of the plasmonic chip. Striped rectangles 1 and 2 are the SPP launchers as shown in (A). The groove doublet forms a plasmonic BS. The characterized splitter gives $T_1 = 29 \pm 1\%$ and $R_1 = 18 \pm 1\%$ when shining from coupler 1 and $T_2 = 32 \pm 1\%$ and $R_2 = 15 \pm 1\%$ when shining from coupler 2. For both input ports, the losses of the BS are measured to be approximately 53%. The SPPs propagate from launcher 1 or 2 to the BS and finally reach the large slits (black rectangles) where they are converted into photons in the silica substrate. (**C**) Line shape of the sample. It exhibits how an SPP can be generated with a Gaussian beam focused orthogonally to the photon-to-SPP converter. The SPP reaches the grooves of the plasmonic BS and finally propagates to the slit. The slit allows the SPP to couple out as photon in the substrate at 42° with an efficiency of about 50%.

to efficiently couple a normally incident Gaussian beam into directional SPPs. Details concerning the SPP launchers can be found in a preliminary report (*29*). The launched SPPs from couplers 1 and 2 are then combined with a plasmonic symmetric splitter made of two identical grooves oriented at 45°. The width, depth, and spacing of the splitter grooves are 350, 150, and 250 nm, respectively. Finally, the SPPs are decoupled by the two large strip slits on the rear side of the sample to avoid any contamination of the detected photons by straight light resulting from the backscattering at the front side of the sample. Calculation evidences that the decoupling efficiency is 50% for 10-µm-wide slits and that the decoupled photons propagate in the glass at an oblique angle of 42° (Fig. 1C) with a parallel momentum approximately equal to the parallel momentum of the surface plasmons. The single chip has a total footprint of 40×40 µm^2. The dimension is compatible with experimental requirements for interfacing free-space photons and SPPs. In addition, the 10-µm separation distance between all the plasmonic components guarantees that the amplitudes of quasi-cylindrical waves that are either directly scattered by the SPP launcher at the splitter level or generated by the splitter at the strip-slit level (*30*) are at least 10 times smaller than the SPP amplitudes. Thus, the plasmonic chip, despite its compactness, provides a true test of the bosonic character of SPPs. We collected the output signal from the substrate of the sample with an appended solid immersion lens, and we coupled it to avalanche photodiodes (APDs) connected to multimode fibers. We measured the transmission and reflection factors of the as-fabricated plasmonic BS depending on the input port. For coupler 1, we obtained $T_1 = 29 \pm 1\%$ and $R_1 = 18 \pm 1\%$. For coupler 2, we measured $T_2 = 32 \pm 1\%$ and $R_2 = 15 \pm 1\%$. The losses were equivalent for both ports and were measured to be approximately 53%. We note that the BS factors are unbalanced as a result of the variations of the actual BS dimensions with respect to the simulated BS dimensions. The losses, when propagating along the plasmonic sample, are evaluated to be 2.5%, and, eventually, only 0.1% of the photons emitted by the source do reach detectors A and B (see section S2).

Particle behavior of the single surface plasmon

We used the plasmonic device to launch and characterize the single SPP with antibunching (Fig. 2A). The box at the top left symbolizes the heralded single-photon source with its two outputs. We denote R_C as the rate of the heralding pulse. A heralded single horizontally polarized photon is sent to a half-wave plate (HWP0), which rotates the linear polarization of the photon falling onto a polarizing beam splitter (PBS) cube. This allows us to choose between the plasmonic HBT and MZ configurations later on. Each output mode of the PBS is focused on a photon-to-SPP coupler on the plasmonic chip. The SPP modes are recombined with the plasmonic splitter, and each output is converted back to photons using the slits. The output signals are collected on APDs A and B. When the neutral axis of HWP0 is aligned with those of the PBS, the photon is transmitted and focused on a single coupler of the plasmonic sample. This configuration is analogous to the HBT experiment with heralded single SPPs. The intensity autocorrelation function at zero delay time $g^{(2)}(0)$ for SPPs is obtained by measuring the heralded outcoupled photon rates from the chip on APDs A ($R_{A|C}$) and B ($R_{B|C}$) while varying the pump power on the crystal. Because the losses between the crystal and the detection events on APDs A and B are huge, we measured $g^{(2)}(0)$ by integrating the counts over a 20-min period. Near the origin, $g^{(2)}(0)$ can be approximated in a linear regime (see section S3) as

$$g^{(2)}(0) \approx 2\mu\Delta T \tag{1}$$

where $\Delta T = 10$ ns is the resolution gate time for the coincidence measurement and µ is the intrinsic emission rate of the source of photons without taking into account the heralding efficiency leading to R_C. The heralded antibunching measurement is shown in Fig. 2B. We note that $g^{(2)}(0)$ is clearly below the classical limit. $g^{(2)}(0)$ down to 0.03 ± 0.06 is a clear indication that the source emits SPPs one by one (*25*), and each of them is either transmitted or reflected by the BS but never both at the same time. This antibunching illustrates the particle-like behavior of the single SPP.

Wave behavior of the single surface plasmon

Next, we made a single SPP interference experiment. We set the pump power to reach $g^{(2)}(0) = 0.25$. This value establishes a good compromise between the signal-to-noise ratio, which is deteriorated

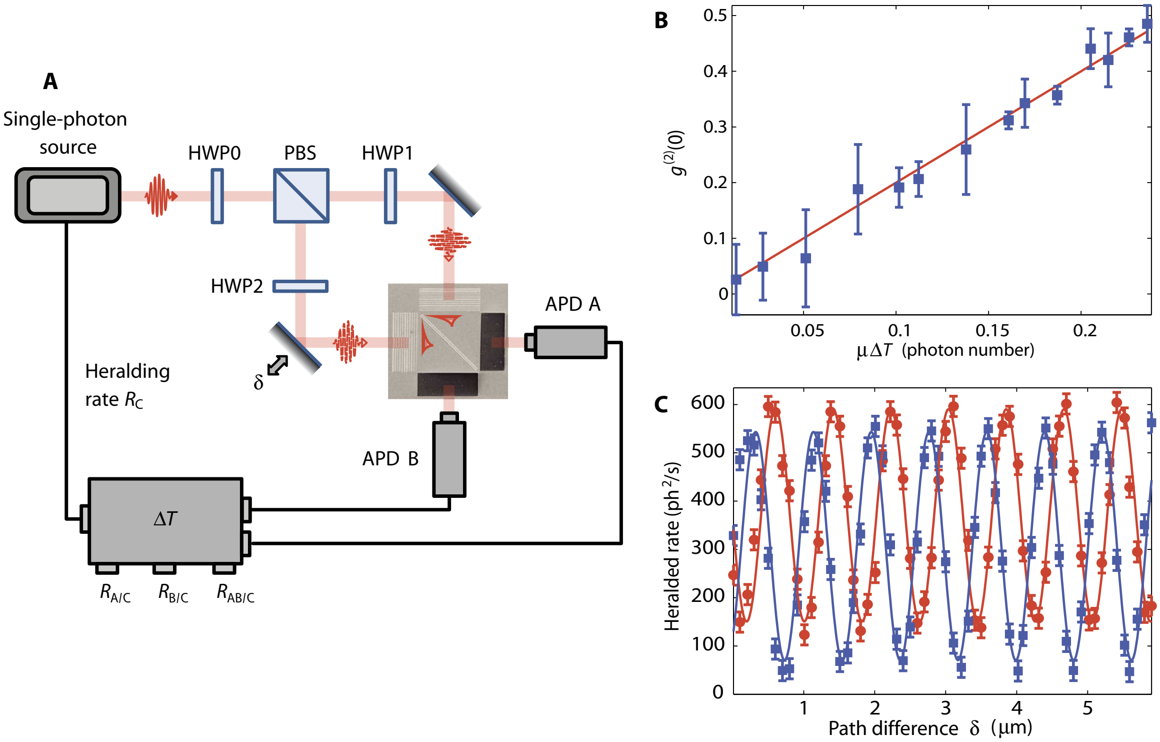

Fig. 2. Experiments on SSPs showing the unicity of the SPP state and its wave behavior. (**A**) Sketch of the SPP experiments. The orientation of the first half-wave plate (HWP0) determines the polarization state impinging on the PBS cube and allows choosing between the HBT and MZ configurations of the SPP setup. HWP1 and HWP2 are half-wave plates that control the polarization of the incident beams on the photon-to-SPP couplers. For both experiments, we recorded the heralding rate R_C and the heralded rates $R_{A|C}$, $R_{B|C}$, and $R_{AB|C}$. (**B**) Intensity correlation function at zero delay $g^{(2)}(0)$ as a function of the mean photon number produced in the gating window $\Delta T = 10$ ns. The lowest measured value of $g^{(2)}(0)$ obtained is 0.03 ± 0.06, which is well below the classical limit and is a signature of a single SPP state. The data points were obtained with 20 min of integration. (**C**) The single SPP source was used at $g^{(2)}(0) = 0.25$ to perform interferences in an MZ interferometer for SPPs. We plotted the heralded photon output rates $R_{A|C}$ (red circles) and $R_{B|C}$ (blue squares) of the MZ interferometer for a varying delay in one arm of the interferometer. The solid lines are the sine fit functions of our experimental data.

by the instability of the interferometer for long acquisition times and the quality of the source to ensure about 90% chance to obtain single SPP events. In the setup described in Fig. 2A, we now sent 45°-polarized photons on the PBS. The output state of the PBS is thus a balanced superposition of the output photonic modes, each of which illuminates one of the plasmon-photon coupler. After conversion to SPPs, the superposition of the two plasmonic modes recombines onto the plasmonic splitter. The two outputs of the plasmonic BS are then converted back to photons that are collected on APDs A and B. The setup is now equivalent to an MZ interferometer where a delay δ is adjusted mechanically by elongating one arm with respect to the other. We selected the heralded output signals of the MZ interferometer ($R_{A|C}$ and $R_{B|C}$) and plotted them as a function of the delay δ (Fig. 2C). We observed interference fringes located in an exponentially decaying envelope as the delay increases in one arm of the MZ interferometer, which is the signature of a wave behavior from the SPP. From this envelope, we find that the spectral width is not modified, showing that there is no dephasing process associated with the SPP conversion and propagation. At the central position of the envelope, we obtain a maximal visibility [$V = (R_{max} - R_{min})/(R_{max} + R_{min})$] of 62 ± 3% for output A and 79 ± 2% for output B. The difference between the visibilities can be explained by the imperfections of the setup (see section S2). There is also a phase difference of 120° between the two outputs of the MZ interferometer. With a lossless symmetric BS, we would have expected the outputs to be in opposition of phase as energy conservation applies. However, because of the losses in the BS, the phase shift can be different from π. Performing a rigorous numerical simulation of the experiment, we found agreement between the experiment and the simulations for the relative positions of the fringes on the two outputs A and B (section S4). Although losses are detrimental for some quantum effects such as the visibility of the Hong-Ou-Mandel experiment (*20*, *27*), they can be used as a resource for manipulating plasmonic interferences, even in the deep quantum regime involving one- or two-plasmon states (*31*).

DISCUSSION

Here, we have developed a platform to manipulate SPPs in a controlled way using directional plasmonic couplers, large-slit decouplers, and a two-groove BS. On the one hand, we have measured the intensity correlation function of heralded SPPs and observed single SPP antibunching in the low-intensity pump regime of the source. This is evidence of a particle-like behavior. On the other hand, we observed fringes by making those single SPPs interfere in an MZ interferometer, therefore showing their wavelike nature. We found that the interferences produced by the plasmonic chip differ from the photonic case. The observed phase difference has been attributed to the subtle role of losses in the interferometer. Despite the losses, the quantum properties of the SPP statistics have been preserved. We thus demonstrated the wave-particle duality of nonguided, freely propagating SPPs.

MATERIALS AND METHODS

Sample fabrication

We used 300-nm-thick gold films deposited on clean glass substrates by e-beam evaporation (ME300 Plassys system) at a pressure of 2×10^{-6} mbar and at a rate of 0.5 nm/s. Their root mean square roughness is 1 nm. They were then loaded in a crossbeam Zeiss Auriga system and milled by a focused ion beam at low current (20 pA), except for the large slits used to decouple plasmons for propagating light that were milled at 600 pA.

Experimental method

The single-photon source was based on parametric down-conversion in a potassium titanyl phosphate crystal (KTP crystal from Raicol). It generated pairs of 806-nm degenerate photons. The combination of the pair source with the heralded detection of one photon of the pair formed the single-photon source. A tunable laser diode (Toptica) with an extended cavity was focused by a 300-mm focal-length plano-convex lens on a periodically poled KTP crystal at 38 mW with a 60-μm waist. We used the laser diode at 403 nm to emit degenerate pairs at 806 nm, and the laser diode's temperature was maintained at 32.5°C. The waist in the crystal was conjugated to infinity with a 100-mm focal-length plano-convex lens, and the red photons emerging from the crystal were separated in polarization by a PBS cube (Fichou Optics). We eliminated the remaining pumping signal with an interferometer filter from AHF (FF01-810/10). The photons were coupled to polarization-maintaining monomode fibers (P1-780PM-FC) via collimators (F220FC-780, Thorlabs). Each photon was outcoupled via Long Working Distance M Plan Semi-Apochromat microscope objectives (LMPLFLN-20× BD, Olympus) and sent to two different outputs of a PBS (Fichou Optics) with orthogonal polarizations. They left the cube by the same output port and were focused with a 10× microscope objective (Olympus) on the plasmonic sample. The plasmonic sample was mounted on a solid immersion lens. The surface plasmons propagating on the chip left the sample by two different output slits. The conversion of the SPP back to photons via the slits led to two different directions of light in free space. The photons from the output ports could be collected from the rear side of the sample using mirrors and a 75-mm focal-length lens for each output. The output modes were then conjugated to multimode fibers via a 10× microscope objective (Olympus), which were connected to single-photon counting modules (SPCMs).

Detection method

All the photons in these experiments were sent to SPCMs, which deliver transistor-transistor logic pulses. APDs A and B are PerkinElmer modules (SPCM AQRH-14), and APD C is a Laser Component SPCM (Count-100C-FC). To count the correlations between the heralding signal and the APD A and B pulses, we used a PXI Express system from National Instruments (NI). The NI system is composed of a PXIe-1073 chassis on which NI FlexRIO materials are plugged: a field-programmable gate array (FPGA) chip (NI PXIe-7961R) and an adapter module at 100 MHz (NI 6581). The FPGA technology allows changing the setting of the acquisition by simply programming the FPGA chip to whatever set of experiments we want to conduct. A rising edge from APD C triggers the detection of another rising edge on channel A or B or both at specific delays. Counting rates and correlations of heralded coincidences between channels A and B are registered. The resolution of the detection system is mainly ruled by the acquisition board frequency clock at 100 MHz, which corresponds to a time resolution of 10 ns.

SUPPLEMENTARY MATERIALS

Supplementary material for this article is available at http://advances.sciencemag.org/cgi/content/full/2/3/e1501574/DC1

Section S1. Characterization of the single-photon source.

Section S2. Characterization of the plasmonic chip.

Section S3. Fit function for HBT experiments.

Section S4. The lossy BS influence on the MZ interferences.

Fig. S1. Single-photon source antibunching.

Fig. S2. Schematic of the lossless-lossy MZ interferometer.

Fig. S3. Reflection and transmission coefficients of the plasmonic BS as a function of the incidence angle.

Fig. S4. Comparison between experimental data and numerical simulation of the plasmonic MZ outputs.

References (*32*, *33*)

REFERENCES AND NOTES

1. P. Grangier, G. Roger, A. Aspect, Experimental evidence for a photon anticorrelation effect on a beam splitter: A new light on single-photon interferences. *Europhys. Lett.* **1**, 173–179 (1986).
2. C. K. Hong, L. Mandel, Experimental realization of a localized one-photon state. *Phys. Rev. Lett.* **56**, 58–60 (1986).
3. W. Neuhauser, M. Hohenstatt, P. E. Toschek, H. Dehmelt, Localized visible Ba^+ mono-ion oscillator. *Phys. Rev. A* **22**, 1137–1140 (1980).
4. D. E. Chang, V. Vuletić, M. D. Lukin, Quantum nonlinear optics—Photon by photon. *Nat. Photonics* **8**, 685–694 (2014).
5. A. Goban, C.-L. Hung, S.-P. Yu, J. D. Hood, J.A. Muniz, J. H. Lee, M. J. Martin, A. C. McClung, K. S. Choi, D. E. Chang, O. Painter, H. J. Kimble, Atom–light interactions in photonic crystals. *Nat. Commun.* **5**, 3808 (2014).
6. M. S. Tame, K. R. McEnery, Ş. K. Özdemir, J. Lee, S. A. Maier, M. S. Kim, Quantum plasmonics. *Nat. Phys.* **9**, 329–340 (2013).
7. D. Pines, *Elementary Excitations in Solids: Lectures on Phonons, Electrons, and Plasmons* (W. A. Benjamin, New York, 1963).
8. M. S. Tame, C. Lee, J. Lee, D. Ballester, M. Paternostro, A. V. Zayats, M. S. Kim, Single-photon excitation of surface plasmon polaritons. *Phys. Rev. Lett.* **101**, 190504 (2008).
9. A. Archambault, F. Marquier, J.-J. Greffet, C. Arnold, Quantum theory of spontaneous and stimulated emission of surface plasmons. *Phys. Rev. B* **82**, 035411 (2010).
10. J. M. Elson, R. H. Ritchie, Photon interactions at a rough metal surface. *Phys. Rev. B* **4**, 4129–4138 (1971).
11. A. V. Akimov, A. Mukherjee, C. L. Yu, D. E. Chang, A. S. Zibrov, P. R. Hemmer, H. Park, M. D. Lukin, Generation of single optical plasmons in metallic nanowires coupled to quantum dots. *Nature* **450**, 402–406 (2007).
12. R. Kolesov, B. Grotz, G. Balasubramanian, R. J. Stöhr, A. A. L. Nicolet, P. R. Hemmer, F. Jelezko, J. Wrachtrup, Wave–particle duality of single surface plasmon polaritons. *Nat. Phys.* **5**, 470–474 (2009).
13. E. Altewischer, M. P. van Exter, J. P. Woerdman, Plasmon-assisted transmission of entangled photons. *Nature* **418**, 304–306 (2002).
14. J. S. Fakonas, A. Mitskovets, H. A. Atwater, Path entanglement of surface plasmons. *New J. Phys.* **17**, 023002 (2015).
15. S. Fasel, M. Halder, N. Gisin, H. Zbinden, Quantum superposition and entanglement of mesoscopic plasmons. *New J. Phys.* **8**, 13 (2006).
16. S. Fasel, F. Robin, E. Moreno, D. Erni, N. Gisin, H. Zbinden, Energy-time entanglement preservation in plasmon-assisted light transmission. *Phys. Rev. Lett.* **94**, 110501 (2005).
17. A. Huck, S. Smolka, P. Lodahl, A. S. Sørensen, A. Boltasseva, J. Janousek, U. L. Andersen, Demonstration of quadrature-squeezed surface plasmons in a gold waveguide. *Phys. Rev. Lett.* **102**, 246802 (2009).

18. A. G. Curto, G. Volpe, T. H. Taminiau, M. P. Kreuzer, R. Quidant, N. F. van Hulst, Unidirectional emission of a quantum dot coupled to a nanoantenna, *Science* **329**, 930–933 (2010).
19. B. Ji, E. Giovanelli, B. Habert, P. Spinicelli, M. Nasilowski, X. Xu, N. Lequeux, J.-P. Hugonin, F. Marquier, J.-J. Greffet, B. Dubertret, Non-blinking quantum dot with a plasmonic nanoshell resonator, *Nat. Nanotechnol.* **10**, 170–175 (2015).
20. Y.-J. Cai, M. Li, X.-F. Ren, C.-L. Zou, X. Xiong, H.-L. Lei, B.-H. Liu, G.-P. Guo, G.-C. Guo, High-visibility on-chip quantum interference of single surface plasmons. *Phys. Rev. Appl.* **2**, 014004 (2014).
21. J. S. Fakonas, H. Lee, Y. A. Kelaita, H. A. Atwater, Two-plasmon quantum interference. *Nat. Photonics* **8**, 317–320 (2014).
22. R. W. Heeres, L. P. Kouwenhoven, V. Zwiller, Quantum interference in plasmonic circuits. *Nat. Nanotechnol.* **8**, 719–722 (2013).
23. G. Di Martino, Y. Sonnefraud, M. S. Tame, S. Kéna-Cohen, F. Dieleman, Ş. K. Özdemir, M. S. Kim, S. A. Maier, Observation of quantum interference in the plasmonic Hong-Ou-Mandel effect. *Phys. Rev. Appl.* **1**, 034004 (2014).
24. G. Fujii, D. Fukuda, S. Inoue, Direct observation of bosonic quantum interference of surface plasmon polaritons using photon-number-resolving detectors, *Phys. Rev. B* **90**, 085430 (2014).
25. R. Loudon, *The Quantum Theory of Light* (Oxford Univ. Press, New York, 2000).
26. H. Paul, Photon antibunching. *Rev. Mod. Phys.* **54**, 1061–1102 (1982).
27. S. M. Barnett, J. Jeffers, A. Gatti, R. Loudon, Quantum optics of lossy beam splitters. *Phys. Rev. A* **57**, 2134–2145 (1998).
28. E. Silberstein, P. Lalanne, J.-P. Hugonin, Q. Cao, Use of grating theories in integrated optics. *J. Opt. Soc. Am. A* **18**, 2865–2875 (2001).
29. A. Baron, E. Devaux, J.-C. Rodier, J.-P. Hugonin, E. Rousseau, C. Genet, T. W. Ebbesen, P. Lalanne, Compact antenna for efficient and unidirectional launching and decoupling of surface plasmons. *Nano Lett.*, **11** 4207–4212 (2011).
30. X. Y. Yang, H. T. Liu, P. Lalanne, Cross conversion between surface plasmon polaritons and quasicylindrical waves. *Phys. Rev. Lett.* **102**, 153903 (2009).
31. J. Jeffers, Interference and the lossless lossy beam splitter. *J. Mod. Opt.* **47**, 1819–1824 (2000).
32. A. Fedrizzi, T. Herbst, A. Poppe, T. Jennewein, A. Zeilinger, A wavelength-tunable fiber-coupled source of narrowband entangled photons. *Opt. Express* **15**, 15377–15386 (2007).
33. O. Alibart, D. B. Ostrowsky, P. Baldi, S. Tanzilli, High-performance guided-wave asynchronous heralded single-photon source. *Opt. Lett.* **30**, 1539–1541 (2005).

Acknowledgments: We acknowledge E. Rousseau, F. Cadiz, and N. Schilder for their help in the beginning of this study, as well as L. Jacubowiez, A. Browaeys, and P. Grangier for fruitful discussions. **Funding:** The research was supported by a DGA-MRIS (Direction Générale de l'Armement–Mission Recherche et Innovation Scientifique) scholarship, by RTRA (Réseau Thématique de Recherche Avancée) Triangle de la Physique, and by a public grant overseen by the French National Research Agency (ANR) as part of the "Investissements d'Avenir" program (reference: ANR-10-LABX-0035, Labex NanoSaclay). J.-J.G. is a senior member of Institut Universitaire de France. **Author contributions:** P.L., G.M., F.M., and J.-J.G. initiated the project. The plasmonic chip design and multiphoton characterization were supervised by P.L. J.-C.R. and J.-P.H. designed the chip, which was fabricated by E.D. and T.W.E. and characterized by A.B. and M.-C.D. M.-C.D. built the setup and performed all quantum experiments under the supervision of G.M. and F.M. M.-C.D., F.M., G.M., and J.-J.G. wrote the paper. All authors discussed the results. **Competing interests:** The authors declare that they have no competing interests. **Data and materials availability:** All data needed to evaluate the conclusions in the paper are present in the paper and/or the Supplementary Materials. Additional data related to this paper may be requested from F.M. (francois.marquier@ institutoptique.fr).

Submitted 4 November 2015
Accepted 7 January 2016
Published 11 March 2016
10.1126/sciadv.1501574

Citation: M.-C. Dheur, E. Devaux, T. W. Ebbesen, A. Baron, J.-C. Rodier, J.-P. Hugonin, P. Lalanne, J.-J. Greffet, G. Messin, F. Marquier, Single-plasmon interferences. *Sci. Adv.* **2**, e1501574 (2016).